The requirement of GW182 in miRNA-mediated gene silencing in *Drosophila* larval development

Eriko Matsuura-Suzuki[1,2], Kaori Kiyokawa[1,3], Shintaro Iwasaki[2,4], Yukihide Tomari[1,4 †]

[1] Institute for Quantitative Biosciences, The University of Tokyo, Bunkyo-ku, Tokyo 113-0032, Japan

[2]RNA Systems Biochemistry Laboratory, RIKEN Cluster for Pioneering Research, Wako, Saitama 351-0198, Japan

[3]Institute of Industrial Science, The University of Tokyo, Meguro-ku, Tokyo 153-8505,

[4]Department of Computational Biology and Medical Sciences, Graduate School of Frontier Sciences, The University of Tokyo, Bunkyo-ku, Tokyo 113-0032, Japan

[†]Correspondence: tomari@iqb.u-tokyo.ac.jp (Y.T.)

Keywords

GW182/microRNA/gene silencing/development/*Drosophila melanogaster*

Abstract

microRNAs (miRNAs) regulate a wide variety of biological processes by silencing their target genes. Argonaute (AGO) proteins load miRNAs to form RNA-induced silencing complex (RISC), which mediates translational repression and/or mRNA decay of the targets. A scaffold protein called GW182 directly binds AGO and the CCR4-NOT deadenylase complex, initiating the mRNA decay reaction. Although previous studies have demonstrated the critical role of GW182 in cultured cells as well as in cell-free systems, its biological significance in living organisms remains poorly explored, especially in *Drosophila melanogaster*. Here, we generated *gw182*-null flies using the CRISPR/Cas9 system and found that, unexpectedly, they can survive until an early second instar larval stage. Moreover, in vivo miRNA reporters can be effectively repressed in *gw182*-null first instar larvae. Nevertheless, *gw182*-null flies have defects in the expression of chitin-related genes and the formation of the larval trachea system, preventing them to complete the larval development. Our results highlight the importance of both GW182-dependent and -independent silencing mechanisms in vivo.

Introduction

microRNAs (miRNAs) are small non-coding RNAs of ~22 nucleotide (nt) in length, which silence the expression of target genes and regulate a wide variety of biological processes. miRNAs are loaded into a member of the Argonaute (AGO) protein family to form the effector ribonucleoprotein complex called RNA-induced silencing complex (RISC). miRNA-loaded RISC binds to complementary target sites, typically located within the 3' untranslated region (3' UTR) of mRNAs, and induces translational repression and/or mRNA deadenylation/decay (Bartel, 2018; Iwakawa & Tomari, 2022). In *Drosophila melanogaster*, miRNAs mainly function through Ago1-containing RISC, whereas small interfering RNAs (siRNAs), another class of small RNAs crucial for silencing of viruses and transposons, function through Ago2-containing RISC (Ghildiyal *et al*, 2008; van Rij *et al*, 2006; Kawamura *et al*, 2008)

Many AGO proteins associate with GW182 as a partner protein, which plays an important role in miRNA-mediated gene silencing. The N-terminal glycine/tryptophan (GW) repeats of GW182 directly binds the three hydrophobic pockets (tryptophane-binding pockets) in the PIWI domain of AGO proteins (Schirle *et al*, 2014; Elkayam *et al*, 2017). GW182 further recruits the CCR4-NOT deadenylase complex and the PAN2-PAN3 deadenylase complex, mainly through its C-terminal region called the "silencing domain" (Jonas & Izaurralde, 2015). Agreeing with the role of GW182 as the scaffold between AGO and the deadenylase complexes, previous studies have demonstrated the essential requirement of GW182 in miRNA-mediated deadenylation and decay of target mRNAs (Braun *et al*, 2011; Chekulaeva *et al*, 2011; Fabian *et al*, 2011; Fukaya & Tomari, 2011). On the other hand, translational repression by miRNAs is reported to occur in two different—GW182-dependent and -independent—manners, at least in cultured cells and in cell-free systems (Fukaya & Tomari, 2012; Fukaya *et al*, 2014; Fukao *et al*, 2014; Jonas & Izaurralde, 2015; Kuzuoğlu-Öztürk *et al*, 2016). However, the physiological importance of GW182 and its modes of action in vivo remain poorly explored.

Multiple GW182 paralogs (TNRC6A, B, and C in humans) exist in many species. *Caenorhabditis elegans* have two GW182 paralogs, AIN-1 and AIN-2, but only AIN-1 can associate with the deadenylase complexes (Ding *et al*, 2005; Zhang *et al*, 2007; Kuzuoglu-Öztürk *et al*, 2012). Importantly, loss of both AIN genes does not cause significant lethality at the embryonic stage, although it later leads to a larval developmental arrest (Jannot *et al*, 2016). Moreover, the embryonic lethality caused by the loss of ALG-1 and ALG-2, two miRNA-specific AGOs in *C. elegans*, can be rescued by a tryptophan-binding pocket mutant of ALG-1, which cannot associate with AIN-1 or AIN-2 (Jannot *et al*, 2016). Moreover, in the germline of

C. elegans, AIN-1 is dispensable but instead the DEAD-box helicase GLH-1 (a homolog of fly Vasa) is required for miRNA-mediated gene regulation (Dallaire *et al*, 2018). These studies strongly suggest that GW182 is not essential for some biological contexts in *C. elegans*. In contrast to worms, *Drosophila melanogaster* has only one GW182 gene called *gawky* (*gw*). Gawky protein (called fly GW182 thereafter) is 1,384 aa in length and binds Ago1, the miRNA-specific AGO in flies. *gw182* gene locates in the tiny 4th chromosome, which lacks crossovers during meiosis and is thus difficult to genetically manipulate. Indeed, gw^1 is the only mutant fly allele reported in the literature so far (Schneider *et al*, 2006). gw^1 expresses a truncated GW182 protein (1–966 aa), which is also detectable in healthy heterozygous adults and thus does not seem to have dominant-negative effects. Yet, homozygous gw^1 mutant embryos fail to cellularize and die before gastrulation. This phenotype of gw^1 is, oddly, even severer than that of a null allele of *ago1*, which becomes lethal only after segment formation of embryos (Kataoka *et al*, 2001). These observations raise the possibility that the specific truncated form of GW182 and/or additional mutation(s) in the gw^1 allele causes the secondary effect, highlighting the necessity of generating and characterizing bona fide *gw182*-null flies to understand its physiological role.

Here, we utilized the CRISPR-Cas9 system and successfully knocked out the *gw182* gene in the challenging 4th chromosome. We found that, unlike gw^1, *gw182*-null flies can survive until an early point of the second instar larval stage. Moreover, in vivo reporters can be effectively silenced in *gw182*-null first instar larvae. Nonetheless, our RNA-seq analysis revealed that *gw182*-null flies have defects in the expression of chitin-related genes and the formation of the larval trachea system, explaining their failure to complete the larval development. Our results highlight the in vivo importance of both GW182-dependent and -independent silencing mechanisms by miRNAs.

Results

Development of an in vivo reporter that can monitor the miR-8 activity in flies

To accurately monitor the silencing activity of fly miRNAs in vivo, we set up a new reporter system with multiple controls. We designed a set of fluorescent reporters under the control of the GAL4-UAS system, a general method to activate gene expression in a tissue- and/or development-specific manner in flies (Brand & Perrimon, 1993). The first GFP reporter includes two copies of a typical, centrally-bulged miR-8 target site in the 3' UTR (the Sensor reporter; Figure 1A and B). As a negative control, the second GFP reporter harbors two copies of mutated miR-8 sites with mismatches in the "seed" region, which is critical for miRNA target recognition (the Mutated reporter; Figure 1A and B). Together with either the Sensor or Mutated GFP reporter, we co-expressed an independent mCherry reporter without miRNA target sites as an internal control and normalized the GFP expression by the mCherry expression (Figure 1A).

We expressed these reporters using an eye-specific driver, *GMR*-GAL4, with or without overexpression of miR-8 (Figure 1C and D). Since endogenous miR-8 is not expressed in the eye disc at the third instar larval stage, the GFP fluorescence of the Sensor reporter remained unsilenced and was readily detectable in the eye disc (Figure 1C and D). Upon miR-8 overexpression, however, the GFP intensity of the Sensor reporter was significantly downregulated, while the mCherry fluorescence of the internal control reporter was unaffected (Figure 1C and D). In contrast to the Sensor reporter, the GFP fluorescence of the Mutated reporter was expectedly observed regardless of the overexpression of miR-8 (Figure 1C and D). miR-8-specific silencing of the Sensor GFP reporter, but not the Mutated reporter, was also confirmed at the mRNA level (Figure 1E). These results demonstrate that this reporter system can accurately monitor the miR-8 silencing activity in living flies.

Ago1-RISC can repress the miR-8 reporter independently of GW182 in the eye disc

We next investigated the impact of GW182 on miRNA-mediated silencing in vivo. We knocked down *gw182* or *ago1* using corresponding inverted repeats (IRs) as the source of dsRNAs to trigger RNA interference (RNAi) (Dietzl *et al*, 2007; Perkins *et al*, 2015) and evaluated the expression levels of the Sensor reporter or the Mutated reporter in the presence or absence of miR-8 in the eye disc of the third instar larvae. qRT-PCR-based quantification of *gw182* or *ago1* mRNA from the dissected eye disc showed only a modest decrease by the corresponding RNAi (Figure EV1A and B), presumably due to inevitable contamination of the surrounding

tissues. Nevertheless, both *gw182* and *ago1* RNAi in the eye disc caused a rough eye phenotype in adult flies associated with miRNA dysfunction, suggesting the knockdown was functionally effective (Figure EV1C). As expected, depletion of *ago1*, but not depletion of *ago2*, abrogated miR-8-dependent silencing of the Sensor reporter both at the protein level (Figure 2A and C, and Figure EV2A and B) and mRNA level (Figure 2D and Figure EV2C), confirming that miR-8 acts through Ago1-RISC. In contrast, the Sensor reporter remained silenced upon knockdown of *gw182* using two independent IRs (Figure 2A, C, D, and Figure EV2). As a control, the Mutated reporter was insensitive to *ago1* or *gw182* knockdown (Figure 2B–D and Figure EV2). These results raise the possibility that AGO1-RISC can silence miRNA targets independently of GW182 in the fly eye disc.

GW182 is required for larval development only after an early second instar stage

In general, residual proteins can remain upon IR-mediated knockdown and it is difficult to exclude their contribution (Figure EV1A and S1B). Therefore, we sought to generate *gw182*-null alleles using the CRISPR-Cas9 system (Gratz *et al*, 2013) and designed a single guide RNA (sgRNA) that targets the first exon of the *gw182* gene (Figure 3A). Despite its challenging genomic location in the tiny 4th chromosome, we successfully obtained two independent mutant alleles (called $gw^{null\text{-}1}$ and $gw^{null\text{-}2}$ thereafter). These alleles had a small deletion that leads to a premature stop codon in the coding sequence of *gw182* (Figure 3B and 3C), which is expected to block the translation of all known functional domains of GW182 and cause nonsense-mediated mRNA decay. Unlike the previously reported phenotype of gw^{1}, homozygous embryos of $gw^{null\text{-}1}$ or $gw^{null\text{-}2}$ completed embryogenesis and hatched normally (Figure 3D). However, most of $gw^{null\text{-}1}$ or $gw^{null\text{-}2}$ larvae died after molting into second instars, at ~50 h after egg laying (Figure 3D). It has been demonstrated that maternally deposited GW182 starts to decline at 60–70 min after embryo laying (Schneider *et al*, 2006). Although the fate of materially deposited GW182 after 60–70 min in unknown, the time point of death of *gw182*-null flies is more than 48 hours after this time window. In the surviving first instar larvae of $gw^{null\text{-}1}$ and $gw^{null\text{-}2}$, only trace amounts of GW182 protein were detectable (Figure 3E). These results suggest that flies can survive embryogenesis and first instar larval development even after maternal GW182 is mostly depleted, but GW182 becomes essential for development at an early second instar stage.

We then performed a series of rescue experiments using $gw^{null\text{-}2}$, which has a larger genomic deletion and is thus more convenient for genotyping than $gw^{null\text{-}1}$. The developmental arrest in $gw^{null\text{-}2}$ was fully rescued by the expression of full-length GW182 driven by the

endogenous promoter of *gw182*. A GW182 fragment (1–605), which lacks the entire silencing domain, could partially rescue the lethality at the second instar larval stage (Figure 3F), agreeing with a previous notion that functional domains of fly GW182 are not exclusively localized to the silencing domain but rather dispersed throughout the protein (Fukaya & Tomari, 2011). A longer GW182 fragment (1–940 aa), which is shorter than the truncated GW182 expressed in gw^{1} (1–966 aa) but was previously shown to largely retain the silencing activity in a cell-free system (Fukaya & Tomari, 2011), could rescue the lethality not only at the second instar stage but also partly at the third instar stage (Figure 3F). These results together imply that the severe embryonic lethal phenotype previously reported for gw^{1} (Schneider *et al*, 2006) is likely caused by a secondary mutation(s) in the genome (also see Discussion).

GW182 is not required for silencing the miR-8 reporter at the first instar stage

To confirm that miRNAs can silence the miR-8 reporter in the absence of GW182 (Figure 2), we crossed $gw^{null\text{-}2}$ with the reporter strains and monitored their expression levels at the first instar larval stage before they die (Figure 3D). Because miR-8 is highly expressed from embryo to larval stages (Ruby *et al*, 2007), we expressed the Sensor reporter or the Mutated reporter using the promotor sequence of miR-8. The Sensor reporter, but not the Mutated reporter, is thus repressed by endogenous miR-8 in this assay (Figure EV3). We found that repression of the Sensor reporter relative to the Mutated reporter was comparable between $gw^{null\text{-}2}$–/– homozygotes and $gw^{null\text{-}2}$–/+ heterozygotes, both at the protein (Figure 4A and 4B) and mRNA (Figure 4C) levels. We concluded that miR-8 can silence the in vivo reporter independently of GW182 in first instar larvae, although it is formally possible that the residual amount of GW182 in $gw^{null\text{-}2}$ is sufficient to support the full silencing activity.

GW182 is required for repression of some endogenous miRNA targets

Although repression of the miR-8 reporter did not apparently require GW182 in first instar larvae (Figure 4), *gw182*-null flies stopped growing and died after molting into second instar larvae (Figure 3D). Thus, it is expected that some endogenous genes are misregulated in the absence of GW182. To explore this possibility, we performed RNA sequencing (RNA-seq) of $gw^{null\text{-}2}$ homozygous larvae at the first instar stage, right before they show developmental arrest, using *yw* larvae as a control. Because miR-8 and miR-14 are the two most abundant miRNAs in fly larvae (Ruby et al., 2007), we focused our transcriptome analysis on mRNAs bearing predicted target sites for miR-8 and miR-14. As expected, miR-8 and miR-14 targets were slightly but significantly upregulated in $gw^{null\text{-}2}$ flies, compared to mRNAs that lack any

predicted target sites for the top 10 abundant larval miRNAs (Figure 5A). Among all upregulated transcripts in *gw*$^{null\text{-}2}$ flies, the predicted targets for miR-8 and miR-14 and those for the top 10 miRNAs accounted for ~15% and ~25%, respectively (Figure 5B). The expression levels of miR-8 and miR-14 themselves were comparable or even slightly higher in *gw*$^{null\text{-}2}$ than in *yw* (Figure 5C), indicating that the upregulation of miR-8 and miR-14 targets is due to defects in target repression, rather than the absence of those miRNAs. Similar results were obtained in the comparisons between *gw*$^{null\text{-}2}$–/– and –/+ siblings and between *gw*$^{null\text{-}2}$–/– and +/+ siblings (Figure EV5). Thus, GW182 is required for the proper regulation of at least some miRNA targets.

GW182 is required for the regulation of chitin-related genes and the formation of the larval trachea system

To further investigate the biological role of fly GW182 in vivo, we focused our RNA-seq analysis on protein-coding genes that are differently expressed between *yw* and *gw182*-null mutants at the first instar larval stage. There were many misregulated genes in the two *gw182*-null flies compared to *yw* (Figure 6A–D), while the gene expression profiles were highly similar in *gw*$^{null\text{-}1}$ and *gw*$^{null\text{-}2}$ flies as expected (Figure 6E). Using stringent criteria ($\log_2$FC [fold change] > 1 or < –1; FDR [false discovery rate] < 0.05), we found that 358 and 575 genes were enriched or depleted in *gw*$^{null\text{-}1}$ (Figure 6A and B) and 480 and 612 genes in *gw*$^{null\text{-}2}$, respectively (Figure 6C and D). Of these, 292 enriched genes and 386 depleted genes were shared by *gw*$^{null\text{-}1}$ and *gw*$^{null\text{-}2}$. Gene Ontology (GO) analysis of those commonly misregulated genes showed that genes upregulated in *gw182*-null larvae are associated with defense response to Gram-positive bacterium, peptidoglycan metabolic, peptidoglycan catabolic, and glycosaminoglycan catabolic processes (Figure 6F and EV4A), suggesting that the immune system of *gw182*-null mutants is more sensitive than that of *yw*. Since fly larvae are typically cultured on food that contains raw yeast, a Gram-positive fungus (Bianchi, 1965), we first predicted that excess immune response to yeast may be responsible for the lethality of *gw182*-null flies. However, when we cultured *gw182*-null larvae on yeast-free food, they still showed developmental arrest at the early second instar stage (E.M., K.K., Y.T., unpublished observations). Therefore, we next focused on the GO terms of downregulated genes in *gw182*-null flies and detected strong enrichment of chitin-based cuticle development and cuticle development genes (Figure 6F and EV4B). It is well known that chitin microfibril is required for the formation of body cuticle, trachea epithelial tube, and gut epithelium, protecting flies from invading pathogens and other harmful stresses (Moussian, 2010). Moreover, downregulated genes in *gw182*-null mutants included *vermiform*

(*verm*), *serpentine* (*serp*) and *mummy* (*mmy*) (Figure 6A and C), whose strong genetic associations with the formation of trachea epithelial tube have been demonstrated (Luschnig *et al*, 2006; Wang *et al*, 2006; Tonning *et al*, 2006). We thus examined the trachea trunks of first instar larvae of $gw^{null\text{-}2}$ and *yw* under microscopy. In *yw* larvae, we could clearly observe two thick trachea trunks with air-filled respiratory tubules (Figure 7A). In contrast, the trachea trunks of $gw^{null\text{-}2}$ larvae were overall thin and showed frequent air-filling defects (Figure 7B). These results indicate that GW182 regulates trachea formation during larval development.

Discussion

In this study, we utilized the CRISPR/Cas9 system and successfully generated *gw182*-null flies. We found that *gw182*-null flies can complete the embryogenesis and develop into second instar larvae. GW182 protein as well as *gw182* mRNA is known to be maternally deposited, which starts to decline at 60–70 min after egg deposition (Schneider *et al*, 2006). Therefore, GW182 may well be required for very early embryogenesis in flies. Nevertheless, it is remarkable that *gw182*-null first instar larvae, in which expression of GW182 is only marginally detectable (Figure 3E), can survive and molt into second instars. This phenotype is much milder than *ago1* null flies (Kataoka *et al*, 2001), implying the existence of an Ago1-dependent but GW182-independent silencing mechanism by miRNAs in vivo, as reported in *C. elegans* (Jannot *et al*, 2016). Indeed, we found that the in vivo miR-8 reporter can be effectively silenced in *gw182*-null first instar larvae (Figure 4) as well as in the GW182-depleted eye disc of third instar larvae (Figure 1). On the other hand, *gw182*-null flies showed developmental arrest at an early second instar stage with misregulation of some miRNA targets (Figure 3D and Figure 5A), suggesting that a GW182-dependent silencing mechanism is essential for survival after this developmental stage. It has been shown that, in *C. elegans*, somatic miRNAs are dependent on GW182 (AIN-1), whereas germline miRNAs function through another factor, GLH-1 (Dallaire *et al*, 2018). Although additional studies are required, it is tempting to speculate that *Drosophila* also utilize a similar tissue-specific or developmental stage-specific dependency on GW182 for miRNA-mediated gene regulation.

It was previously reported that gw^1 homozygous mutants, which express the 1–966 aa fragment of GW182, fail to cellularize at early embryogenesis (Schneider *et al*, 2006). This phenotype of gw^1 is severer than that of *gw182*-null flies (Figure 3D). Moreover, we found that the developmental arrest of *gw182*-null flies at the third instar larvae can be rescued not only by the full-length GW182 but also largely by the 1–940 aa fragment of GW182 (Figure 3F). These observations imply that the phenotype of gw^1 is caused by a secondary mutation(s). The gw^1 mutant has two identified nucleotide changes in the genome: W967stop in *gw* and N144I in the N-terminal region of *myoglianin (myo)*. Myo is a homolog of vertebrate Myostatin (Mstn/GDf8), a member of transforming growth factor (TGF) family (Hinck *et al*, 2016). Mstn circulates in blood as a latent complex with the N-terminal prodomain associated with the ligand domain, and proteolytic cleavage is required to release the active ligand domain from the N-terminal prodomain. Since N144 is placed in the N-terminal prodomain of Myo, the N144I mutation is believed not to affect the function of mature Myo. However, it is possible that the mutation

blocks the proteolytic cleavage and interferes with its function, which may explain the severe phenotype of gw^{1}. Further investigations are needed to clarify this point.

Our RNA-seq analysis suggested that chitin-related genes such as *verm*, *serp* and *mmy* are all downregulated in the first instar larvae of $gw^{null\text{-}1}$ *and* $gw^{null\text{-}2}$ (Figure 6A and C). Chitin is an essential component of larval epidermis, gut, and trachea (Lehane, 1997; Luschnig *et al*, 2006; Wang *et al*, 2006; Hegedus *et al*, 2009). Indeed, *gw182*-null mutants showed defective trachea structures in first instar larvae (Figure 7), demonstrating the importance of GW182 in trachea formation. However, those chitin-related genes do not seem to be direct targets of miRNAs, because miRNA target genes are generally upregulated by the loss of GW182. On the other hand, *ribbon (rib)*, a BTB family transcriptional activator/repressor (Silva *et al*, 2016), was upregulated in *gw182*-null mutants (Figure 6A and C). Rib is considered as a regulating factor of *verm* and *serp*, and it has been demonstrated that proper trachea formation requires Rib (Bradley & Andrew, 2001; Shim *et al*, 2001; Luschnig *et al*, 2006), suggesting a possibility that *verm* and *serp* are misregulated via *rib* in *gw182*-null flies. Future studies are warranted to clarify the relationship between miRNA targets and their associated genes that regulate trachea formation.

Materials and Methods

Drosophila strains

Fly culture and crosses were carried out at room temperature. *miR-8-GAL4* strain (#104917) and w^{1118}*; PBac(681.P.FSVS-1)PMCA*^{CPTI001995} (#115256) were obtained from Kyoto *Drosophila* Genomics and Genetics Resource Center. *GMR-GAL4* strain (#9146), *ago1*-IR strain [y^1 v^1*; P(TRiP.HM04006)attP2* (#31700)] and *ago2-IR* [y^1 *sc** v^1 sev^{21}*; P{TRiP.HMS00108}attP2* (#34799)] is obtained from Bloomington Stock Center. *gw-IR(1)* strains [w^{1118}*; P(GD10428)v45772* (#v45772)] and *gw-IR(2)* [*P*(KK101472)*VIE-260B* (#v103581)] were obtained from Vienna *Drosophila* Resource Center. *M(UAS-mir-8.S)ZH-86Fb* (#F001944) was obtained from FlyORF. w^{1118}*;ln(4)Ci*^{D}, *Ci*^{D}*panCi*^{D}*/Dp(2;4)ey*^{D}, *Alpey*^{D}*:ey*^{D} was a kind gift from Tetsuya Tabata (The University of Tokyo).

Generation of reporter transgenic flies

The UAS-MCS-K10 3' UTR region of pUASp (Rørth, 1998) was amplified by PCR and then inserted into the pBS vector using NEBuilder HiFi DNA Assembly Master Mix (NEB) to generate pBS-UASp. For the internal control, the mCherry sequence amplified by PCR from pmCherry (Clontech) was inserted into pBS-UASp (pBS-UASp-mCherry). Subsequently, the UASp-mCherry-K10 3' UTR region of pBS-UASp-mCherry was amplified by PCR and inserted into pattB vector to generate pattB-UASp-mCherry. For the Sensor and Mutated GFP reporters, the corresponding miR-8 target sequence was inserted downstream of GFP in pAcGFP (Clontech) using the XhoI/NotI restriction enzyme site. Then, a DNA fragment containing GFP with the miRNA target sequence was inserted into pBS-UASp using the KpnI/SpeI restriction enzyme site (pBS-UASp-GFP-miRNA). Next, a fragment of UASp-GFP-miRNA target site was amplified from pBS-UASp-GFP-miRNA by PCR and inserted into pattB-UASp-mCherry to create pattB-UASp-GFP-miRNA-UASp-mCherry. To obtain reporter transgenic lines, pattB-UASp-GFP-miRNA-UASp-mcherry was injected into fly embryos in which phiC31 integrase is expressed in the germline (*y[1] w[1118]; PBac{y[+]-attP-3B}VK00002*, #9723 Bloomington Stock Center) (BestGene Inc.). F0 flies were crossed with *yw* and F1 progeny with red-eye color was balanced by *CyO*.

Antibodies

Rabbit anti-GW182 antibody was generated by immunizing His-tagged recombinant GW182 (1

−1061 aa) and the antisera were affinity-purified using a Protein A column (MBL). Mouse monoclonal anti-AGO1 antibody was a kind gift from Mikiko Siomi. Rabbit DYDDDDK Tag antibody was purchased from Cell Signaling (2368S).

Immunohistology

Eye discs of third instar larvae were dissected in PBS, fixed in 2% formaldehyde, 0.1% TritonX-100 containing PBS at 25°C for 20 min, and then washed three times in PBS containing 0.1% Tween 20 (PBST) at 25 °C for 5 min each. After blocking with PBST containing 10% donkey serum at 25°C for one hour, eye discs were incubated with the primary antibodies, anti-GFP (1:100) (MBL) and anti-mRFP (1:100) (MBL) in PBST containing 10% donkey serum at 4°C overnight, followed by washing in PBST three times. The eye discs were then incubated with the secondary antibodies conjugated with fluorescein, Alexa488 (1:200) (Thermofisher), or Alexa596 (1:200) (Thermofisher) for two hours at 25 °C. The eye discs were washed in PBST and mounted in Vectashield antifade mounting medium (Vector Laboratories). Confocal microscopy was carried out on FV3000 confocal laser scanning system (Olympus) and the fluorescence intensity was assessed with Fiji software. *P*-values were calculated by Student's t-test (unpaired, two-sided) or one-way ANOVA with the post hoc Tukey HSD test with R or Excel. In Figure 2C, 4B, EV2b and EV3b, *P*-values were below the lower limit of the statistical calculation software, hence the exact value cannot be shown.

qRT-PCR

Total RNA was purified from eye discs or first instar larvae by FastGene RNA Basic Kit (Nippon Genetics). The cDNA was synthesized by using PrimeScript RT reagent Kit (TAKARA) using the random hexamer. qRT-PCR was performed by TB Green Premix Ex Taq II (TAKARA) using gene specific primers and Thermal Cycler Dice Real Time System (TAKARA). The sequences of gene specific primer set were shown as follows: *GFP*, 5' - CAA CAT CGA GGA TGG CAG CGT -3' and 5' - CAT GTG ATC GCG CTT CTC GTT G -3' ;*mCherry*, 5' - GAA CGG CCA CGA GTT CGA GA -3' and 5' - CTT GGA GCC GTA CAT GAA CTG AGG -3' ; *rp49*, 5' - CAC CAG TCG GAT CGA TAT GCT AAG -3' and 5' - GTA ACC GAT GTT GGG CAT CAG A -3' ; *gw182*, 5' - CTG CTT ACA CTG ATC TGG TCC AAG AGT TT -3' and 5' - CGC TTC CTG GTG TAA TGC TGG GAT CAT CTT -3', *ago-1*, 5' - GCG AGG TTT GGT TCG GTT TC -3' and 5' - CGT TGA TGT CGC GAA TGT CC -3'. For miRNA qPCR, total RNA was purified from first instar larvae by miRNeasy kit (QIAGEN) according to the manufacturer's instruction. For Figure5C, the cDNA was synthesized using

miScript II RT kit (QIAGEN). qRT-PCR was performed by QuantiTect SYBR Green PCR using miRNA-specific primers provided as miScript Universal primer QIAGEN), Dm_miR-8_1 miScript Primer assay (QIAGEN), and Dm_miR-14_1 miScript Primer assay (QIAGEN) and Thermal Cycler Dice Real Time System (TAKARA). For Figure EV5C, the cDNA was synthesized using miRCURY LNA RT Kit (QIAGEN) and qRT-PCR was performed by miRCURY LNA SYBR Green PCR Kit (QIAGEN) and Thermal Cycler Dice Real Time System (TAKARA) with dme-miR-8-3p miRCURY LNA miRNA PCR Assay (QIAGEN), dme-miR-14-3p miRCURY LNA miRNA PCR Assay (QIAGEN), and dme-U6-snRNA custom miRCURY LNA miRNA PCR Assay (QIAGEN). *P*-values were calculated by Student's t-test (unpaired, two-sided) or one-way ANOVA with the post hoc Tukey HSD test with R. In Figure 2D and 4C, *P*-values were below the lower limit of the statistical calculation software, hence the exact value cannot be shown.

Generation of the *gw182*-null alleles

CRISPR/Cas9-mediated knockout of the *gw* locus was performed using the pU6-BbsI-chiRNA plasmid (Addgene # 45946) (Gratz *et al*, 2013). The target site in *gw182 gene* was selected by using CRISPR DESIGN site (http://crispr.mit.edu). The sense and antisense oligonucleotides corresponding to the selected target sequence were annealed and inserted into BbsI-digested pU6-BbsI-chiRNA plasmid. The *gw* chiRNA plasmid was injected into embryos of the y^1 *M(vas-Cas9)ZH2A* w^{1118} strain (BestGene Inc.). Males or females carrying vas-Cas9 and a sgRNA transgene were crossed to W^{1118}; *ln(4)*Ci^D, Ci^D*panCi*^{D}*/Dp(2;4)*ey^D, *Alpey*^{D}*:*ey^D flies. From each progeny, ten flies were isolated and checked for the deletion of *gw* by genome PCR. Eventually seven independent strains that have frameshift mutations in *gw182* were established. In this study, line 1 and 2, which had largest deletion regions, were used and named $gw^{null\text{-}1}$ and $gw^{null\text{-}2}$, respectively.

Genome PCR

Genome DNA from a wing of the heterozygous adult fly of each strain was extracted as follows. A wing was suspended in 5 µl of genome extraction buffer (25mM NaOH, 0.2mM EDTA) and incubated at 95 ºC for 10 min, and then the suspension was neutralized by 5 µl of 150 mM HCl. 2 µl of the extracted genome solution was used as a template for Genome PCR by GoTaq (Promega). The sequences of *gw182* gene specific primer set designed around the CRISPR target site were 5' -GAG TCC AAT TTG AGA AAC GGA GGT CA-3' and 5' - CTG ATC GTT TGC GCT TAA CTT CAT TAA TTC T-3'. The PCR products were analyzed by MultiNA

(SHIMADZU). The PCR fragments that were shorter than that of the wildtype were subcloned into pCR-TOPO (Invitrogen) and sequenced using the M13 forward and reverse primers.

Determination of the lethal stage of *gw182*-null mutants

Eggs of the progeny of $gw^{null\text{-}1}$/*PBac(681.P.FSVS-1)PMCA*^{CPTI001995} or $gw^{nul1\text{-}2}$/*PBac(681.P.FSVS-1)PMCA*^{CPTI001995} were laid on grape juice plates with yeast pastes at 25°C for 2 hours. 26, 50 and 76 hours after egg laying, 88–96 first instar larvae were collected and checked for the genotype by genome PCR. *PBac(681.P.FSVS-1)PMCA*^{CPTI001995}, expressing YFP trapped in the *PMCA* gene on the 4th chromosome (Lowe *et al*, 2014), was used as a marker.

Generation of flies expressing truncated GW182

The genomic region 5,185 bp upstream of the first ATG of *gw182* was cloned and joined with the full-length *gw182* CDS containing FLAG-tag in the C-terminal region, and the 3' UTR. This construct was inserted into the pattB vector [pattB-(GW182-full)-flag]. For the truncated mutants of GW182, the CDS region was replaced by the corresponding GW182 truncated sequences [pattB-(GW182-605)-flag and pattB-(GW182-940)-flag]. In order to obtain transgenic lines, pattB-(GW182-full)-flag, pattB-(GW182-605)-flag or pattB-(GW182-940)-flag was injected into fly embryos in which phiC31 integrase is expressed in the germline (y^1 *M(vas-int.Dm)ZH-2A w*; M(3xP3-RFP.attP')ZH-51C*, #24482 Bloomington Stock Center) (BestGene Inc.). F0 flies were crossed with *yw* and F1 progeny with red eye color was balanced by *CyO*.

Rescue of *gw182*-null allele by GW182 truncated mutants

Females of $gw^{nul1\text{-}2}$/ *ln(4)*Ci^D, $Ci^D panCi^D$ were crossed with males of *GW182-605 (II);* $gw^{null\text{-}2}$/ *ln(4)*Ci^D, $Ci^D panCi^D$ *or GW182-940 (II);* $gw^{null\text{-}2}$/ *ln(4)*Ci^D, $Ci^D panCi^D$ *or GW182-full (II);* $gw^{null\text{-}2}$/ *ln(4)*Ci^D, $Ci^D panCi^D$ *or +/+;* $gw^{null\text{-}2}$/ *ln(4)*Ci^D, $Ci^D panCi^D$ (negative control). The F1 progeny with GW182 transgene was selected based on RFP expression, a marker of the attP site (Bischof *et al*, 2007), at each larval stage. Genome PCR was performed for selected larvae to discriminate homozygote and heterozygote of $gw^{null\text{-}2}$. The sequences of the *gw182* gene-specific primer set were 5' -GAG TCC AAT TTG AGA AAC GGA GGT CA-3' and 5' - CAT TAA TTC TAA TAG ATA TTA GGC CTA -3'. The percentage of rescue was calculated by dividing the number of homozygotes of $gw^{null\text{-}2}$ with a truncated *gw182* transgene by the total number of larvae with the *gw182* transgene.

Western blots and antibodies

For Western blots of *gw182*-null larvae, YFP-negative first instar larvae of the progeny of gw^{null-1}/*PBac(681.P.FSVS-1)PMCA*^{CPTI001995} or gw^{nul1-2}/*PBac(681.P.FSVS-1)PMCA*^{CPTI001995} were collected 38 hr after egg laying and were lysed in Passive lysis buffer (Promega). After centrifugation, proteins were loaded on an 8% polyacrylamide gel and transferred onto a PVDF membrane (Millipore). Chemiluminescence was induced by Luminata Forte Western HRP Substrate (Millipore), and images were acquired by a LAS-3000 imaging system (FujiFilm) or Amersham Imager 600 (GE healthcare). Rabbit anti-GW182 (1:1000), mouse anti-Ago1 (1:1000), and goat anti-*β*-Actin (1:1000, Santa Cruz sc-1615) were used for blotting. *yw* first instar larvae were used as a positive control of GW182 expression.

RNA-seq

First instar larvae were collected and extracted total RNA by RNA basic kit (FastGene) according to the manufacturer protocol. For Figures 5 and 6, total RNA libraries were prepared by using SMART-Seq v4 Ultra® Low Input RNA Kit for Sequencing (Clontech) according to the manufacture's instruction and analyzed by Illumina HiSeq 2500 system (Illumina). For Figure EV5, total RNA libraries were prepared using the Strand-Specific mRNA Library Preparation method by BGI. mRNA was first purified using oligo dT-beads, fragmented, and then used to synthesize cDNA. The resulting double-stranded cDNA fragments underwent end-repair, followed by the addition of a single 'A' nucleotide to the 3' ends of the blunt fragments. Next, adaptors were ligated to the cDNAs, which were subsequently amplified by PCR. Finally, the cDNA library was analyzed using the DNBseq system by MGI Tech.

RNA sequence reads were analyzed on the Galaxy web platform (usegalaxy.eu) (Afgan *et al*, 2018) or by manual commands. After trimming of the adaptor sequence, quality was controlled by FastQC 0.11.2. Reads were mapped to *Drosophila melanogaster* BDGP6.28 genome using STAR (version 2.7.0a) (Dobin *et al*, 2013). For the differential expression analysis at the transcripts level, mapped reads were counted using RSEM (Li & Dewey, 2011). For the differential expression analysis at the gene level, mapped reads were counted using *featureCounts* (Liao *et al*, 2014) by summing the total number of reads overlapping at least 10 nucleotides with the gene annotation, including only uniquely mapped reads in the genome. Differential gene expression and normalized counts as TPM (Transcripts Per Kilobase Million) were calculated using *DESeq2* (Love *et al*, 2014). Genes having > 0 TPM were kept for further analysis. Processed data were transferred to R, then cumulative fractions of fold change values were drawn with the ggplot2 package. The FDR was calculated using the Benjamini and Hochberg method. Target mRNAs of each miRNA were predicted by using TargetScan (Fly,

Release 7.2) (Agarwal *et al*, 2018). Gene ontology analysis was performed using stringent criteria ($\log_2$FC [fold change] > 1 or < –1; FDR [false discovery rate] < 0.05) by GOrilla (Eden *et al*, 2009). The Protein-protein networks in enriched or depleted biological processes were analyzed by STRING (Szklarczyk *et al*, 2019). For Figure 6F, N: the total number of genes. B: the total number of genes associated with a specific GO term. n: the total number of genes in the RNA-seq data. b: the number of genes associated with a specific GO term in the RNA-seq data, shown by color gradient. Enrichment = (b/n) / (B/N), shown by circle size.

Assessment of reporter expression in first instar larvae

First instar larvae were collected after 40−42 hours of hatching and the fluorescence of GFP and mCherry under fluorescence microscopy were observed (Zeiss). Fluorescence intensity was quantified by Fiji software. For each larva, the average fluorescence intensity of GFP or mCherry in the body part of interest was measured and the average of auto-fluorescence of *yw* was subtracted as the background.

Trachea observation

Second instar larvae after 50 hours after egg laying were collected and fixed with 4% Paraformaldehyde/PBST. After washing with PBST, the trachea was observed under microscopy.

Accession numbers

The RNA-seq data obtained in this study (GSE192811 and GSE267756) were deposited to the National Center for Biotechnology Information (NCBI).

Data Availability

The datasets and computer code produced in this study are available in the following databases:
RNA-Seq data: Gene Expression Omnibus GSE192811
(https://www.ncbi.nlm.nih.gov/geo/query/acc.cgi?&acc=GSE192811)
RNA-Seq data: Gene Expression Omnibus GSE267756
(https://www.ncbi.nlm.nih.gov/geo/query/acc.cgi?acc=GSE267756)

Disclosure and competing interest statement

The authors declare that no competing interests exist. Yukihide Tomari is a member of the Advisory Editorial Board of *The EMBO Journal*. This has no bearing on the editorial consideration of this article for publication.

References

Afgan E, Baker D, Batut B, van den Beek M, Bouvier D, Cech M, Chilton J, Clements D, Coraor N, Grüning BA, *et al* (2018) The Galaxy platform for accessible, reproducible and collaborative biomedical analyses: 2018 update. *Nucleic Acids Res* 46: W537–W544

Agarwal V, Subtelny AO, Thiru P, Ulitsky I & Bartel DP (2018) Predicting microRNA targeting efficacy in Drosophila. *Genome Biol* 19: 152

Bartel DP (2018) Metazoan MicroRNAs. *Cell* 173: 20–51

Bianchi DE (1965) DIFFERENTIAL STAINING OF YEAST FOR PURIFIED CELL WALLS, BROKEN CELLS, AND WHOLE CELLS. *Stain Technol* 40: 79–82

Bischof J, Maeda RK, Hediger M, Karch F & Basler K (2007) An optimized transgenesis system for Drosophila using germ-line-specific phiC31 integrases. *Proc Natl Acad Sci U S A* 104: 3312–3317

Bradley PL & Andrew DJ (2001) ribbon encodes a novel BTB/POZ protein required for directed cell migration in Drosophila melanogaster. *Development* 128: 3001–3015

Brand AH & Perrimon N (1993) Targeted gene expression as a means of altering cell fates and generating dominant phenotypes. *Development* 118: 401–415

Braun JE, Huntzinger E, Fauser M & Izaurralde E (2011) GW182 proteins directly recruit cytoplasmic deadenylase complexes to miRNA targets. *Mol Cell* 44: 120–133

Chekulaeva M, Mathys H, Zipprich JT, Attig J, Colic M, Parker R & Filipowicz W (2011) miRNA repression involves GW182-mediated recruitment of CCR4-NOT through conserved W-containing motifs. *Nat Struct Mol Biol* 18: 1218–1226

Dallaire A, Frédérick P-M & Simard MJ (2018) Somatic and Germline MicroRNAs Form Distinct Silencing Complexes to Regulate Their Target mRNAs Differently. *Dev Cell* 47: 239-247.e4

Dietzl G, Chen D, Schnorrer F, Su KC, Barinova Y, Fellner M, Gasser B, Kinsey K, Oppel S, Scheiblauer S, *et al* (2007) A genome-wide transgenic RNAi library for conditional gene inactivation in Drosophila. *Nature* 448: 151–156

Ding L, Spencer A, Morita K & Han M (2005) The developmental timing regulator AIN-1 interacts with miRISCs and may target the argonaute protein ALG-1 to cytoplasmic P bodies in C. elegans. *Mol Cell* 19: 437–447

Dobin A, Davis CA, Schlesinger F, Drenkow J, Zaleski C, Jha S, Batut P, Chaisson M & Gingeras TR (2013) STAR: ultrafast universal RNA-seq aligner. *Bioinformatics* 29: 15–21

Eden E, Navon R, Steinfeld I, Lipson D & Yakhini Z (2009) GOrilla: a tool for discovery and visualization of enriched GO terms in ranked gene lists. *BMC Bioinformatics* 10: 48

Elkayam E, Faehnle CR, Morales M, Sun J, Li H & Joshua-Tor L (2017) Multivalent Recruitment of Human Argonaute by GW182. *Mol Cell* 67: 646-658.e3

Fabian MR, Cieplak MK, Frank F, Morita M, Green J, Srikumar T, Nagar B, Yamamoto T, Raught B, Duchaine TF, *et al* (2011) miRNA-mediated deadenylation is orchestrated by GW182 through two conserved motifs that interact with CCR4-NOT. *Nat Struct Mol Biol* 18: 1211–1217

Fukao A, Mishima Y, Takizawa N, Oka S, Imataka H, Pelletier J, Sonenberg N, Thoma C & Fujiwara T (2014) MicroRNAs trigger dissociation of eIF4AI and eIF4AII from target mRNAs in humans. *Mol Cell* 56: 79–89

Fukaya T, Iwakawa H-O & Tomari Y (2014) MicroRNAs block assembly of eIF4F translation initiation complex in Drosophila. *Mol Cell* 56: 67–78

Fukaya T & Tomari Y (2011) PABP is not essential for microRNA-mediated translational repression and deadenylation in vitro. *EMBO J* 30: 4998–5009

Fukaya T & Tomari Y (2012) MicroRNAs mediate gene silencing via multiple different pathways in drosophila. *Mol Cell* 48: 825–836

Ghildiyal M, Seitz H, Horwich MD, Li C, Du T, Lee S, Xu J, Kittler ELW, Zapp ML, Weng Z, *et al* (2008) Endogenous siRNAs derived from transposons and mRNAs in Drosophila somatic cells. *Science* 320: 1077–1081

Gratz SJ, Cummings AM, Nguyen JN, Hamm DC, Donohue LK, Harrison MM, Wildonger J & O'Connor-Giles KM (2013) Genome engineering of Drosophila with the CRISPR RNA-guided Cas9 nuclease. *Genetics* 194: 1029–1035

Hegedus D, Erlandson M, Gillott C & Toprak U (2009) New insights into peritrophic matrix synthesis, architecture, and function. *Annu Rev Entomol* 54: 285–302

Hinck AP, Mueller TD & Springer TA (2016) Structural Biology and Evolution of the TGF-β Family. *Cold Spring Harb Perspect Biol* 8

Iwakawa HO & Tomari Y (2022) Life of RISC: Formation, action, and degradation of RNA-induced silencing complex. *Mol Cell* 82: 30–43

Jannot G, Michaud P, Quévillon Huberdeau M, Morel-Berryman L, Brackbill JA, Piquet S, McJunkin K, Nakanishi K & Simard MJ (2016) GW182-Free microRNA Silencing Complex Controls Post-transcriptional Gene Expression during Caenorhabditis elegans Embryogenesis. *PLoS Genet* 12: e1006484

Jonas S & Izaurralde E (2015) Towards a molecular understanding of microRNA-mediated gene silencing. *Nat Rev Genet* 16: 421–433

Kataoka Y, Takeichi M & Uemura T (2001) Developmental roles and molecular characterization of a Drosophila homologue of Arabidopsis Argonaute1, the founder of a novel gene superfamily. *Genes Cells* 6: 313–325

Kawamura Y, Saito K, Kin T, Ono Y, Asai K, Sunohara T, Okada TN, Siomi MC & Siomi H (2008) Drosophila endogenous small RNAs bind to Argonaute 2 in somatic cells. *Nature* 453: 793–797

Kuzuoğlu-Öztürk D, Bhandari D, Huntzinger E, Fauser M, Helms S & Izaurralde E (2016) miRISC and the CCR4-NOT complex silence mRNA targets independently of 43S ribosomal scanning. *EMBO J* 35: 1186–1203

Kuzuoglu-Öztürk D, Huntzinger E, Schmidt S & Izaurralde E (2012) The Caenorhabditis elegans GW182 protein AIN-1 interacts with PAB-1 and subunits of the PAN2-PAN3 and CCR4-NOT deadenylase complexes. *Nucleic Acids Res* 40: 5651–5665

Lehane MJ (1997) Peritrophic matrix structure and function. *Annu Rev Entomol* 42: 525–550

Li B & Dewey CN (2011) RSEM: accurate transcript quantification from RNA-Seq data with or without a reference genome. *BMC Bioinformatics* 12: 323

Liao Y, Smyth GK & Shi W (2014) featureCounts: an efficient general purpose program for assigning sequence reads to genomic features. *Bioinformatics* 30: 923–930

Love MI, Huber W & Anders S (2014) Moderated estimation of fold change and dispersion for RNA-seq data with DESeq2. *Genome Biol* 15: 550

Lowe N, Rees JS, Roote J, Ryder E, Armean IM, Johnson G, Drummond E, Spriggs H, Drummond J, Magbanua JP, *et al* (2014) Analysis of the expression patterns, subcellular localisations and interaction partners of Drosophila proteins using a pigP protein trap library. *Development* 141: 3994–4005

Luschnig S, Bätz T, Armbruster K & Krasnow MA (2006) serpentine and vermiform encode matrix proteins with chitin binding and deacetylation domains that limit tracheal tube length in Drosophila. *Curr Biol* 16: 186–194

Moussian B (2010) Recent advances in understanding mechanisms of insect cuticle differentiation. *Insect Biochem Mol Biol* 40: 363–375

Perkins LA, Holderbaum L, Tao R, Hu Y, Sopko R, McCall K, Yang-Zhou D, Flockhart I, Binari R, Shim HS, *et al* (2015) The Transgenic RNAi Project at Harvard Medical School: Resources and Validation. *Genetics* 201: 843–852

van Rij RP, Saleh M-C, Berry B, Foo C, Houk A, Antoniewski C & Andino R (2006) The RNA silencing endonuclease Argonaute 2 mediates specific antiviral immunity in Drosophila melanogaster. *Genes Dev* 20: 2985–2995

Rørth P (1998) Gal4 in the Drosophila female germline. *Mech Dev* 78: 113–118

Ruby JG, Stark A, Johnston WK, Kellis M, Bartel DP & Lai EC (2007) Evolution, biogenesis, expression, and target predictions of a substantially expanded set of Drosophila microRNAs. *Genome Res* 17: 1850–1864

Schirle NT, Sheu-Gruttadauria J & MacRae IJ (2014) Structural basis for microRNA targeting. *Science* 346: 608–613

Schneider, Najand N, Chaker S, Pare JM, Haskins J, Hughes SC, Hobman TC, Locke J & Simmonds AJ (2006) Gawky is a component of cytoplasmic mRNA processing bodies required for early Drosophila development. *J Cell Biol* 174: 349–358

Shim K, Blake KJ, Jack J & Krasnow MA (2001) The Drosophila ribbon gene encodes a nuclear BTB domain protein that promotes epithelial migration and morphogenesis. *Development* 128: 4923–4933

Silva D, Olsen KW, Bednarz MN, Droste A, Lenkeit CP, Chaharbakhshi E, Temple-Wood ER & Jemc JC (2016) Regulation of Gonad Morphogenesis in Drosophila melanogaster by

BTB Family Transcription Factors. *PLoS One* 11: e0167283

Szklarczyk D, Gable AL, Lyon D, Junge A, Wyder S, Huerta-Cepas J, Simonovic M, Doncheva NT, Morris JH, Bork P, *et al* (2019) STRING v11: protein-protein association networks with increased coverage, supporting functional discovery in genome-wide experimental datasets. *Nucleic Acids Res* 47: D607–D613

Tonning A, Helms S, Schwarz H, Uv AE & Moussian B (2006) Hormonal regulation of mummy is needed for apical extracellular matrix formation and epithelial morphogenesis in Drosophila. *Development* 133: 331–341

Wang S, Jayaram SA, Hemphälä J, Senti K-A, Tsarouhas V, Jin H & Samakovlis C (2006) Septate-Junction-Dependent Luminal Deposition of Chitin Deacetylases Restricts Tube Elongation in the Drosophila Trachea. *Curr Biol* 16: 180−185

Zhang L, Ding L, Cheung TH, Dong MQ, Chen J, Sewell AK, Liu X, Yates JR & Han M (2007) Systematic identification of C. elegans miRISC proteins, miRNAs, and mRNA targets by their interactions with GW182 proteins AIN-1 and AIN-2. *Mol Cell* 28: 598–613

Figure Legends

Figure 1. Construction and validation of the miR-8 reporter in eye discs.

(A) Schematic diagrams of reporter constructs bearing GFP with two miR-8 target sites (top) or two seed-mismatched sites (middle), and mCherry without miR-8 target sites as an internal control (bottom).

(B) Schematic representation of the pairing between miR-8 and the Sensor reporter or the Mutated reporter for each miRNA-binding site. Lines represent base pairs.

(C) Fluorescence microscopy of the Sensor reporter or the Mutated reporter in the eye disc of third instar larvae. GFP (green) and mCherry (red) expressions were compared with or without miR-8 overexpression. Scale bar: 20 μm.

(D) Quantification of the relative GFP protein level in Figure 1C. The GFP fluorescence levels were normalized to the mCherry fluorescence levels, and the fold changes are shown relative to the average value without miR-8 overexpression as mean ± SD. Error bars represent standard derivation from independent eye discs for each sample. P-values were determined by Student's t-test (unpaired, two-sided). *, *P*=3.46e-8

(E) Quantification of the relative GFP mRNA level by qRT-PCR for Figure 1C. The GFP mRNA levels were normalized to the mCherry mRNA levels, and the fold changes are shown relative to the value without miR-8 overexpression as mean ± SD. Error bars represent standard derivation from 3 independent experiments. P-values were determined by Student's t-test (unpaired, two-sided). *, *P*=5.37e-3

Genotypes (C–E): *GMR-GAL4/UAS-Sensor reporter; +/+* (n=8), *GMR-GAL4/UAS-Sensor reporter; UAS-miR-8/+* (n=5) , *GMR-GAL4/UAS-Mutated reporter;+/+* (n=10) ,and *GMR-GAL4/UAS-Mutated reporter;UAS-miR-8/+* (n=10) . The numbers (n) are for Figure 1D.

Figure 2. GW182 is not essential for miR-8-mediated silencing of the reporter in eye discs.

(A, B) Fluorescence microscopy images for the Sensor reporter (A) and the Mutated reporter (B) upon miR-8 overexpression. *gw-IR(1)* and *gw-IR(2)* are independent IR-expressing strains, and the indicated genes are knockdown in the third instar larval eye disc. Scale bar: 20 μm.

(C) Quantified derepression at the protein level in Figure 2A and B. The GFP fluorescence level was normalized to the mCherry fluorescence level, and the derepression levels are shown relative to the negative control without IR expression (–) of the Sensor reporter or the Mutated reporter as mean ± SD. Note that eye discs in Figure 2A and 2B were observed with different laser intensities, and the data were normalized to (–) independently. Error bars represent

standard derivation from 10 independent eye discs for each sample. P-values were calculated by one-way ANOVA with the post hoc Tukey HSD test. *, $P < 1.00e-7$

(D) Quantified derepression at the mRNA level in the Sensor and Mutated reporters. GFP mRNA level was normalized to mCherry mRNA level, and the derepression levels are shown relative to the negative control (–) of the Senor reporter as mean ± SD. Error bars represent standard derivation from three independent experiments. P-values were calculated by one-way ANOVA with the post hoc Tukey HSD test. *, P=3.30e-4, **, $P < 1.00e-7$.

Genotypes for A: *GMR-GAL4/UAS-Sensor reporter; UAS-miR-8/+* (n=10), *GMR-GAL4, GW182-IR(1)/UAS-Sensor reporter;UAS-miR-8/+* (n=10), *GMR-GAL4,GMR-IR(2)/UAS-Sensor reporter; UAS-miR-8/+* (n=10), *GMR-GAL4,ago1-IR/UAS-Sensor reporter; UAS-miR-8/+* (n=10). The numbers (n) are for Figure 2C.

Genotypes for B: *GMR-GAL4/UAS-Mutated reporter; UAS-miR-8/+* (n=10), *GMR-GAL4,GW182-IR(1)/UAS-Mutated reporter; UAS-miR-8/+* (n=10), *GMR-GAL4,GMR-IR(2)/UAS-Mutated reporter; UAS-miR-8/+* (n=10), and *GMR-GAL4,ago1-IR/ UAS-Mutated reporter; UAS-miR-8/+* (n=10). The numbers (n) are for Figure 2C.

Figure 3 Generation of *gw182*-null alleles by CRISPR/Cas9 system

(A) A schematic representation of the *gw182* gene and their transcripts showing with the sgRNA target site. Exons are shown as gray boxes, 5'UTR, and 3'UTR as white boxes.

(B) sgRNA target sequence and modified sequences in *gw182*-null alleles. Target site and PAM motif are shown in a pink box and blue box, respectively. The cleaved site by Cas9 is indicated by a black arrowhead.

(C) Domain structure of GW182 protein and mutant proteins expressed in *gw182*-null mutants.

(D) Genotype ratio at each larval stage of the F1 generation of crossing with heterozygotes of *gw182*-null mutants.

(E) Western blots of GW182 and AGO1 in homozygotes of *gw182*-null mutant at first instar larval stage. β-Actin is used as an internal control.

(F) Percentage of rescued *gw182*-null mutant by GW182 truncated transgenes. The total numbers of individual larvae analyzed for each genotype were: negative control (L1: 95, L2: 85, L3: 57), 605 (L1: 118, L2: 89, L3: 136), 940 (L1: 156, L2: 113, L3: 88), and Full (L1: 84, L2: 156, L3: 116).

Figure 4 GW182 are not essential for miRNA-mediated silencing of the sensor reporter at the first instar larval stage.

(A) Fluorescence microscopy of the Sensor reporter and the Mutated reporter at first instar larval stage. GFP (green) or mCherry (red) expressions are compared between heterozygotes (−/+) or homozygote (−/−) of $gw^{null\text{-}2}$. Scale bar: 250 μm.

(B) Quantification of the derepression level for protein in Figure 4A. The fluorescence GFP level of the Sensor reporter or the Mutated reporter ws normalized to the fluorescence mCherry level and the derepression level is shown relative to $gw^{null\text{-}2}$ −/+ of the Sensor reporter as mean ± SD. Error bars represent standard derivation from the number of animals scored (N; see the materials and methods section). P-values were calculated by one-way ANOVA with the post hoc Tukey HSD test. *, P < 1.00e-7; **, P < 1.00e-7.

(C) Quantification of the derepression level for mRNA. The GFP mRNA level of the Sensor reporter or the Mutated reporter wes normalized to the mCherry mRNA level, and the depression level is shown relative to the $gw^{null\text{-}2}$ −/+ of sensor reporter as mean ± SD. Error bars represent standard derivation from the number of animals scored (n; see Materials and Methods). P-values were calculated by one-way ANOVA with the post hoc Tukey HSD test. *, P < 1.00e-7; **, P < 1.00e-7.

Genotypes: *miR-8-GAL4/UAS-Sensor reporter; +/+;* $gw^{null\text{-}2}$/+ (n=42), *miR-8-GAL4/UAS-Sensor reporter; +/+;* $gw^{null\text{-}2}/gw^{null\text{-}2}$ (n=10), *miR-8-GAL4/UAS-Mutated reporter; +/+;* $gw^{null\text{-}2}$/+ (n=47), *and miR-8-GAL4/UAS-Mutated reporter; +/+;* $gw^{null\text{-}2}/gw^{null\text{-}2}$ (n=13). The numbers (n) are for Figure 4B.

Figure 5. Depletion of GW182 impaired miRNA-mediated silencing for endogenous miRNA targets at the first instar larval stage.

(A) Up-regulation of miRNA targets by knockdown of *gw182*. First larvae of *gw182*-null homozygote or *yw* were collected, and their transcriptomes were analyzed by RNA-seq. The fold change values, $gw^{null\text{-}2}/yw$, were calculated for each mRNA. The cumulative fractions of the average fold change values of two independent experiments are shown for the following categories: mRNAs without a target site of the top 10 most abundant miRNAs (gray) and mRNAs with predicted target sites for miR-8 (orange) or miR-14 (green), together with their P-values of the Mann-Whitney U test.

(B) Pie chart showing the percentage of predicted miRNA targets within the transcripts upregulated by *gw182* deletion. The numbers of transcripts in each category are shown in parentheses.

(C) Quantification of microRNA expression. The levels of miR-8 and miR-14 were measured by quantitative RT-PCR from first instar larvae of $gw^{null\text{-}2}$ homozygote or *yw*. *rp49* was used as

a reference. The data were normalized by the miRNA expression level of *yw*, shown as mean ± SD. Error bars represent standard derivation from three independent experiments. P-values were calculated by Student's t-test (unpaired, two-sided). *, P=0.035; **, P=0.029.

Figure 6. GW182 depletion shows the downregulation of genes related to cuticle development

Gene expression comparison of $gw^{null\text{-}1}$ (A, B) or $gw^{null\text{-}2}$ (C, D) with *yw* by RNA-seq. (A, C) Scatter plot (B, D) Volcano plot. The densities of RNA-seq reads on each protein-coding gene were calculated as transcripts per kilobase million (TPM). The average TPM of two biological replicates is shown. Compared to *yw* RNA-seq, genes with log2FC > 1 or log2FC < -1 (FC, fold change) with FDR < 0.05 (FDR, false discovery rate) in $gw^{null\text{-}1}$ or $gw^{null\text{-}2}$ RNA-seq were defined as enriched (red) or depleted (blue), respectively. The numbers of genes in each category (enriched, no difference, depleted) are shown in parentheses.

(E) Gene expression comparison of $gw^{null\text{-}1}$ and $gw^{null\text{-}2}$ by RNA-seq and scatter plot. The densities of RNA-seq reads on each protein-coding gene were calculated as transcripts per kilobase million (TPM). The average TPM of two biological replicates is shown. Compared to $gw^{null\text{-}1}$ RNA-seq, genes with log2FC > 1 or log2FC < –1 (FC, fold change) with FDR < 0.05 (FDR, false discovery rate) in $gw^{null\text{-}2}$ RNA-seq were defined as enriched (red) or depleted (blue), respectively. The numbers of genes in each category (enriched, no difference, depleted) are shown in parentheses.

(F) Significantly enriched GO (Gene Ontology) categories among genes that are enriched or depleted in $gw^{null\text{-}1}$ and $gw^{null\text{-}2}$. The GO categories (FDR < 0.05) that are common between $gw^{null\text{-}1}$ and $gw^{null\text{-}2}$ are shown. The number of genes associated with a specific GO term in the RNA-seq data is shown by color gradient, and enrichment is shown by circle size. For details, see Materials and Methods.

Figure 7. Deletion of GW182 prevents larval trachea formation

(A) Ventral view of first instar larva of *yw* or $gw^{null\text{-}2}$ homozygote and a magnification of representative air-filling defect of $gw^{null\text{-}2}$ homozygote. Defective air-filling region is indicated by a white bracket.

(B) Percentage of air filling defect of *yw* or $gw^{null\text{-}2}$ homozygote.

Expanded View Figure legends

Figure EV1. Quantification of *gw182* mRNA expression level in *gw182* knockdown flies

(A) Quantification of *gw182* mRNA expression. The *gw182* mRNA levels of two independent *gw182*-IR-expressing strains, *gw-IR(1)* and *gw-IR(2),* at the third instar larval stage were measured by quantitative RT-PCR. *rp49* was used as a reference. The relative expression levels against the control are shown as mean ±□SD. Error bars represent standard derivation from three independent experiments. P-values were calculated by one-way ANOVA with the post hoc Tukey HSD test. *, *P*=0.047.

(B) Quantification of *ago1* mRNA expression. The *ago1* mRNA levels of *ago1-IR*-expressing strains at the third instar larval stage were measured by quantitative RT-PCR. rp49 was used as a reference. The relative expression levels against the control are shown as mean ±□SD. Error bars represent standard derivation from three independent experiments. P-values were calculated by Student's t-test (unpaired, two-sided). *, *P*=0.538.

(C) Rough eye phenotype by *gw182 or ago1* knockdown. The eye phenotypes of two independent *gw182*-IR expressing strains, *gw-IR(1)* and *gw-IR(2),* and *ago1-IR*-expressing strain at the adult stage were observed. *gmr-G4* strain was used as a control.

Genotypes: *GMR-GAL4/+, GMR-GAL4,GW182-IR(1)/+, GMR-GAL4,GW182-IR(2)/+, GMR-GAL4,ago1-IR/+*.

Figure EV2. Ago2 is not essential for miR-8-mediated silencing of the reporter in eye discs.

(A) Fluorescence microscopy images for the Sensor reporter (A) and the Mutated reporter (B) upon miR-8 overexpression. *ago1* or *ago2* was knocked down by corresponding IR in the third instar larval eye disc. Scale bar: 20 µm.

(B) Quantified derepression at the protein level in Figure EV1A. The GFP fluorescence level was normalized to the mCherry fluorescence level, and the derepression levels are shown relative to the negative control without IR expression (–) of the Sensor reporter or the Mutated reporter as mean ±□SD. Error bars represent standard derivation from 10 independent eye discs for each sample. P-values were calculated by one-way ANOVA with the post hoc Tukey HSD test. *, *P*=0.78e-5; **, *P*<1.00e-7.

(C) Quantified derepression at the mRNA level in the Sensor and Mutated reporters. GFP mRNA level was normalized to mCherry mRNA level, and the derepression levels are relative to the negative control (–) of the Sensor reporter, shown as mean ±□SD. Error bars represent standard derivation from 3 independent experiments. P-values were calculated by one-way

ANOVA with the post hoc Tukey HSD test. *, P=4.31e-2; **, P=3.20e-6.

Genotypes: *GMR-GAL4/UAS-Sensor reporter; UAS-miR-8/+* (n=10) , *GMR-GAL4,ago1-IR/UAS-Sensor reporter; UAS-miR-8/+* (n=10), *GMR-GAL4,ago1-IR/UAS-Sensor reporter; UAS-miR-8/ago2-IR* (n=10), *GMR-GAL4/UAS-Mutated reporter; UAS-miR-8/+* (n=10) , *GMR-GAL4,ago1-IR/UAS-Mutated reporter; UAS-miR-8/+* (n=10), *GMR-GAL4,ago1-IR/UAS-Mutated reporter; UAS-miR-8/ago2-IR* (n=10). The numbers (n) are for Figure EV2D.

Figure EV3 The Sensor reporter monitors endogenous miR-8 silencing activity at the larval stage.

(A) Fluorescence microscopy of the Sensor reporter and the Mutated reporter at first instar larval stage. Bright field, GFP (green), or mCherry (red) expressions are compared between *yw*, the Sensor reporter strain, or the Mutated reporter strain. *yw* was used as a negative control. Scale bar: 250 µm.

(B) Quantification of the GFP protein level for Figure EV3A. The fluorescence GFP levels were normalized to the fluorescence mCherry levels, shown as mean ±□SD. Error bars represent standard derivation from three independent larvae for each sample and P-values were calculated by Student's t-test (unpaired, two-sided). *, P<2.2e-16.

Genotypes: *yw, miR-8-GAL4/UAS-Sensor reporter* (n=42) and *miR-8-GAL4/UAS-Mutated reporter* (n=47). The numbers (n) are for Figure EV3B.

Figure EV4 Networks of *gw182*-regulated genes and related biological processes

(A) A protein-protein association network of enriched genes in *gw182*-null mutant and their associated functional classes. Genes classified to defense to gram-positive bacterium, pink; genes classified to peptidoglycan metabolic process, peptidoglycan catabolic process and glycosaminoglycan catabolic process, orange; genes classified to the all above GO terms, red.

(B) A protein-protein association network of depleted genes in *gw182*-null mutant and their associated functional classes. Genes classified to chitin-based cuticle development and cuticle development, lime green; Genes classified to chitin metabolic process, glucosamine-containing compound metabolic process, amino sugar metabolic process, and aminoglycan metabolic process, light blue; genes classified to GO terms represented by light blue and drug metabolic process, aqua green; genes classified to all above GO terms, aqua blue.

Figure EV5 Depletion of GW182 impaired miRNA-mediated silencing for endogenous

miRNA targets at the first instar larval stage, related to Figure 5

(A) Up-regulation of miRNA targets by knockdown of *gw182*. First instar larvae of $gw^{null\text{-}2}$ homozygote, $gw^{null\text{-}2}$ heterozygote or wildtype were collected among siblings, and their transcriptome was analyzed by RNA-seq. The fold change values, $gw^{null\text{-}2}$ homozygote/$gw^{null\text{-}2}$ heterozygote, $gw^{null\text{-}2}$ homozygote/wild type, or $gw^{null\text{-}2}$ heterozygote/wild type were calculated. The cumulative fractions of the average fold change values of two independent experiments are shown for the following categories: mRNAs without a target site of the top 10 most abundant miRNAs (gray) and mRNAs with predicted target sites for miR-8 (orange) or miR-14 (green), together with their P-values of the Mann-Whitney U test. P-values are shown in the figure.

(B) Pie chart showing the percentage of predicted miRNA targets within the transcripts upregulated in $gw^{null\text{-}2}$ homozygote compared to $gw^{null\text{-}2}$ heterozygote or wildtype among siblings. The numbers of transcripts in each category are shown in parentheses.

(C) Quantification of microRNA expression. The relative expression levels of miR-8 and miR-14 were measured by quantitative RT-PCR from first instar larvae of $gw^{null\text{-}2}$ homozygote, $gw^{null\text{-}2}$ heterozygote, or wild type among siblings. *U6 snoRNA* was used as a reference. The data were normalized by the miRNA expression level of wild type, shown as mean ± SD. Error bars represent standard derivation from three independent experiments. P-values were calculated by Student's t-test (unpaired, two-sided). *, *P=0.106;* **, *P=0.092*.

Acknowledgments

We thank all the members of the Tomari laboratories for constructive discussion, technical help, and critical reading of the manuscripts. RNA-sequencing was supported by the IQB central laboratory, The University of Tokyo. This work was supported by JSPS KAKENHI (18H05271 and 21H05278 to Y.T., 21K06026 to E.M.S.), RIKEN Pioneering Project and Aging Project to S.I.

Figure 1

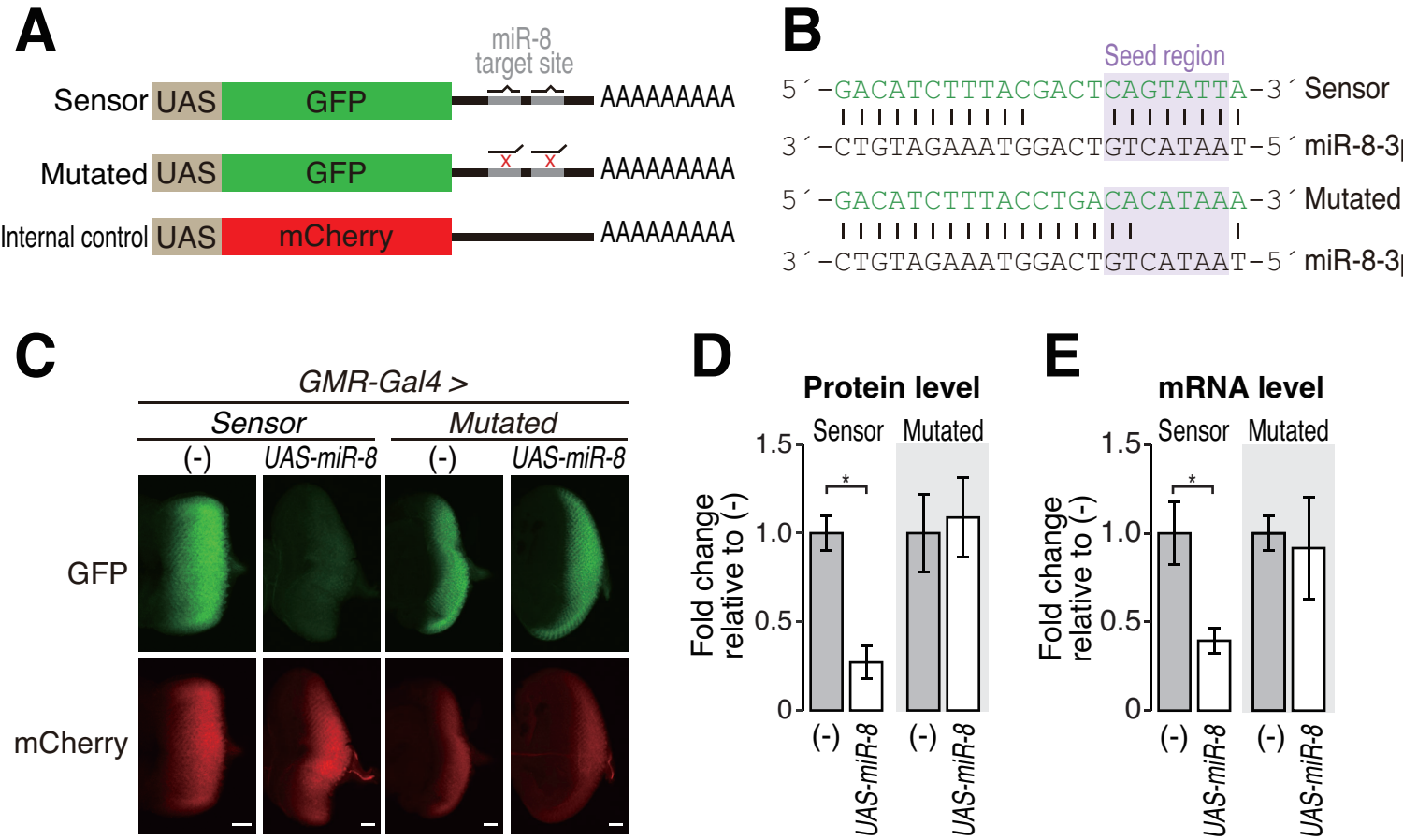

Matsuura-Suzuki et al.

Figure 2

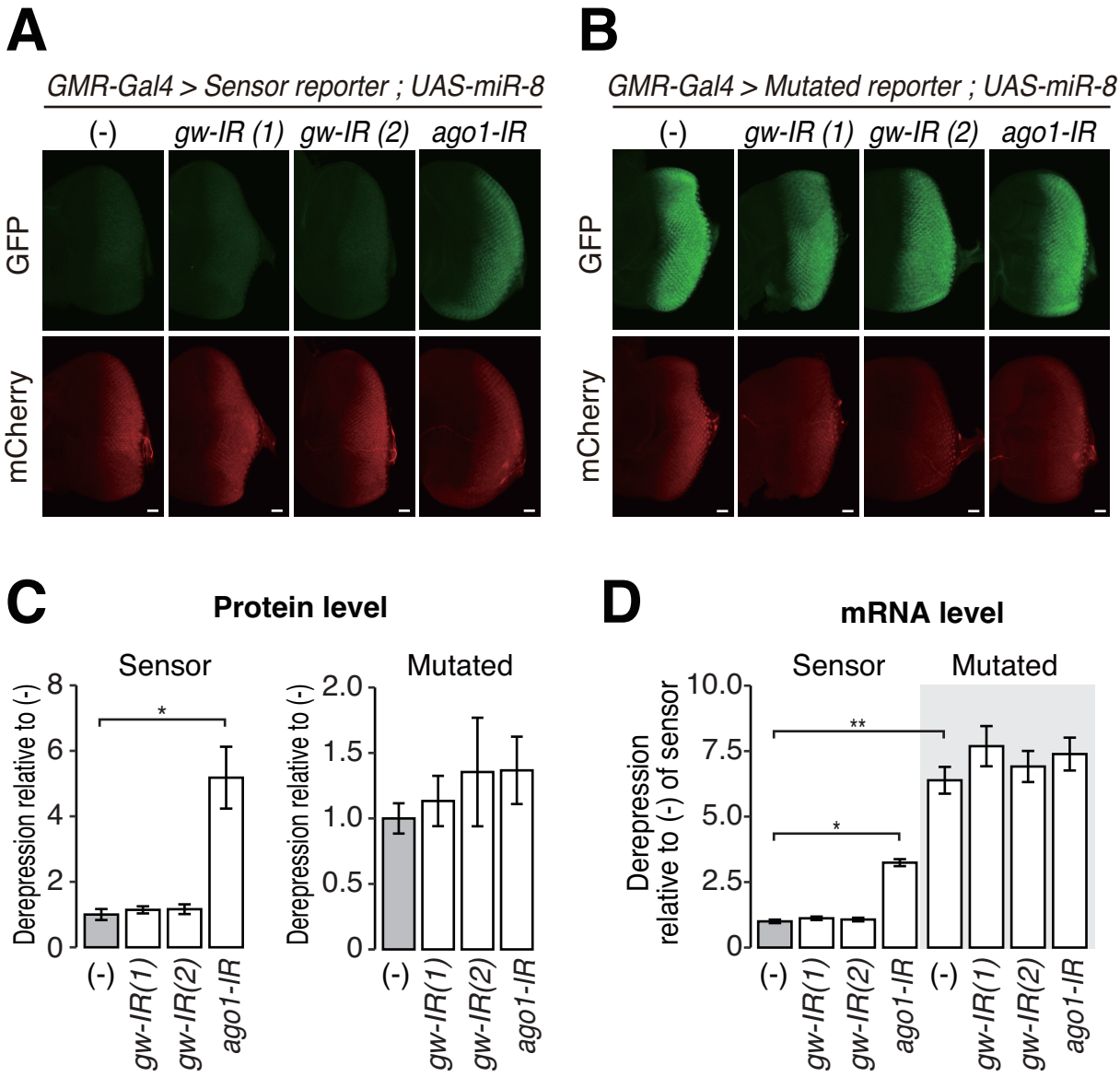
A
GMR-Gal4 > Sensor reporter ; UAS-miR-8
(-)
gw-IR (1)
gw-IR (2)
ago1-IR
GFP
mCherry
B
GMR-Gal4 > Mutated reporter ; UAS-miR-8
(-)
gw-IR (1)
gw-IR (2)
ago1-IR
GFP
mCherry
C
Protein level
Sensor
Mutated
Derepression relative to (-)
0
2
4
6
8
0
0.5
1.0
1.5
2.0
*
(-)
gw-IR(1)
gw-IR(2)
ago1-IR
D
mRNA level
Sensor
Mutated
Derepression relative to (-) of sensor
0
2.5
5.0
7.5
10.0
**
*
(-)
gw-IR(1)
gw-IR(2)
ago1-IR

Figure 3

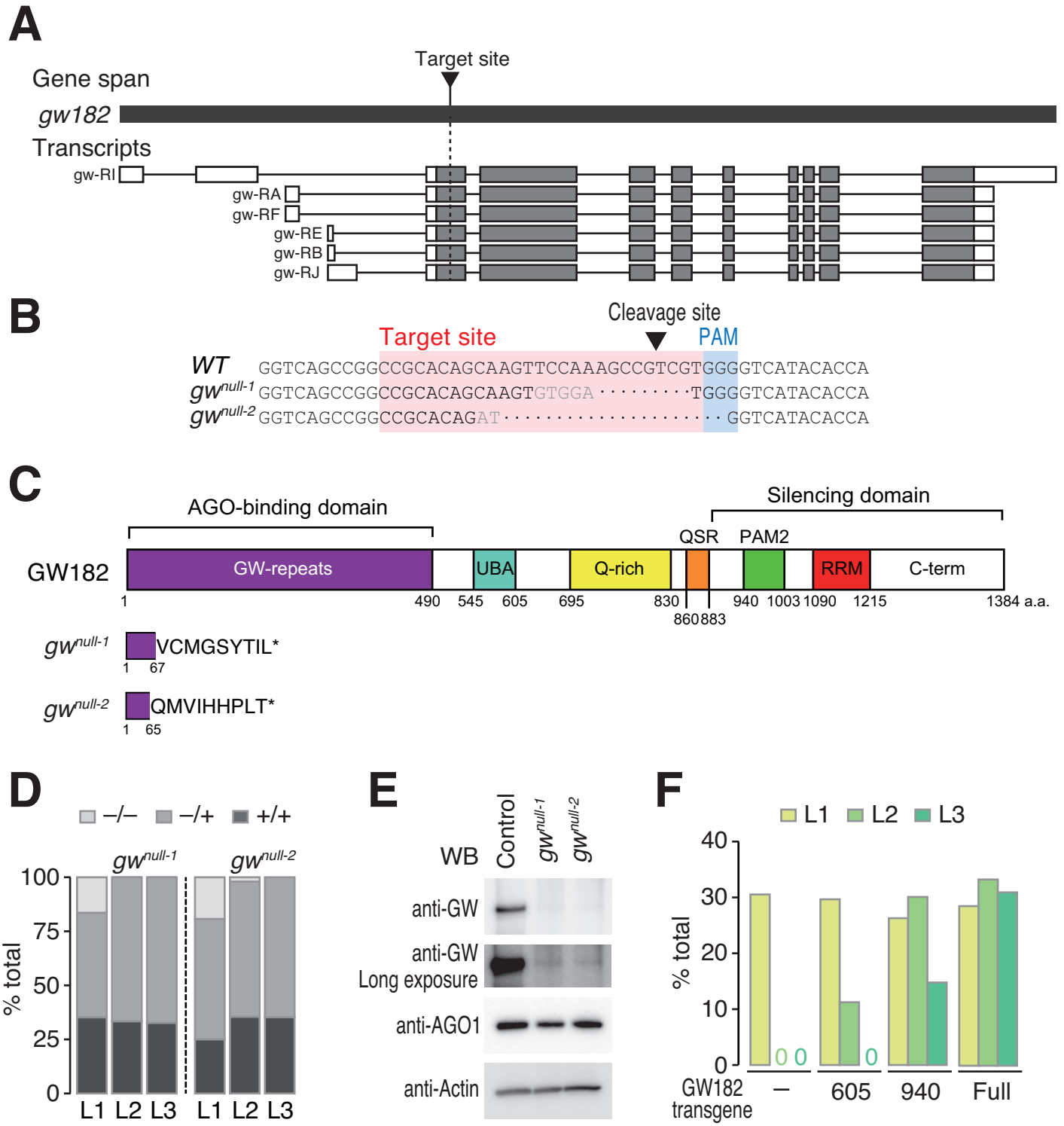

Matsuura-Suzuki et al.

Figure 4

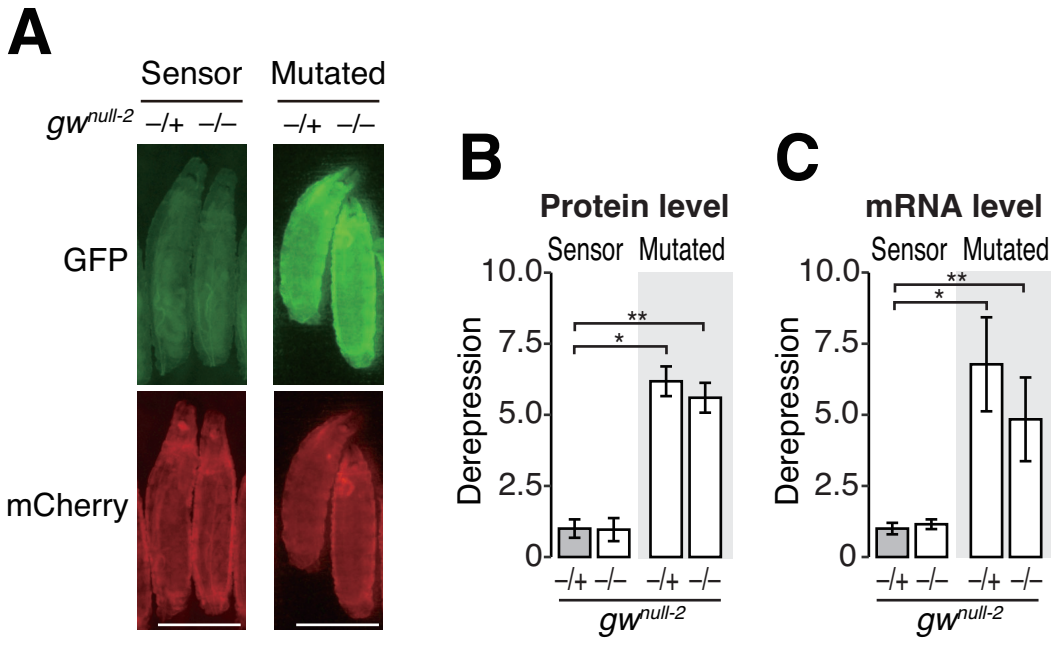
A
Sensor
Mutated
gw^null-2
–/+ –/–
–/+ –/–
GFP
mCherry
B
Protein level
Sensor Mutated
10.0
7.5
5.0
2.5
0
Derepression
**
*
–/+ –/– –/+ –/–
gw^null-2
C
mRNA level
Sensor Mutated
10.0
7.5
5.0
2.5
0
Derepression
**
*
–/+ –/– –/+ –/–
gw^null-2

Figure 5

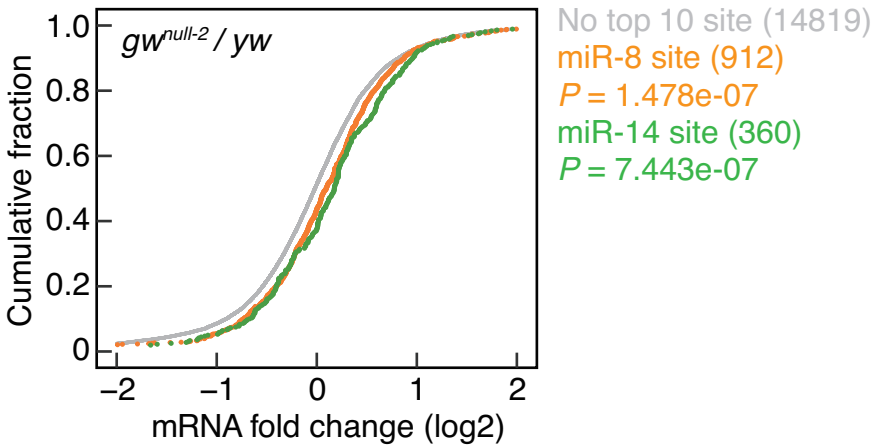
A
gw^null-2 / yw
Cumulative fraction
1.0
0.8
0.6
0.4
0.2
0
−2
−1
0
1
2
mRNA fold change (log2)
No top 10 site (14819)
miR-8 site (912)
P = 1.478e-07
miR-14 site (360)
P = 7.443e-07

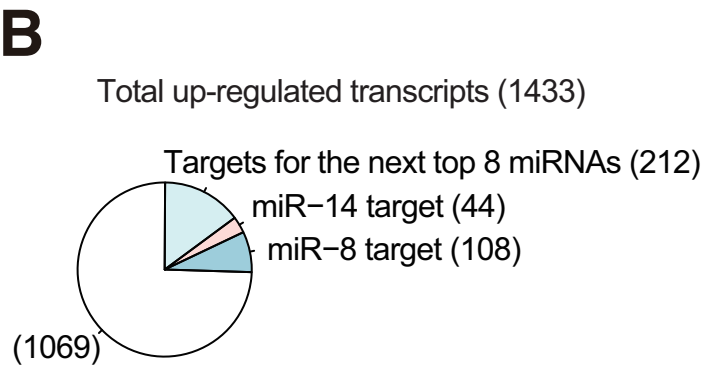
B
Total up-regulated transcripts (1433)
Targets for the next top 8 miRNAs (212)
miR−14 target (44)
miR−8 target (108)
(1069)

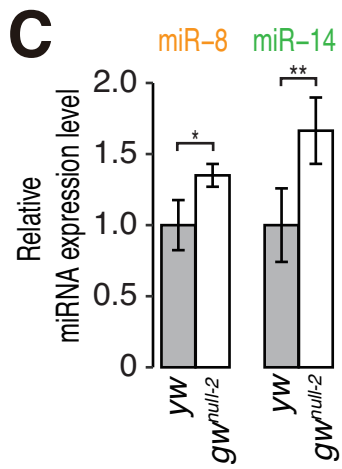
C
miR−8
miR−14
Relative miRNA expression level
2.0
1.5
1.0
0.5
0
*
**
yw
gw^null-2
yw
gw^null-2

Figure 6

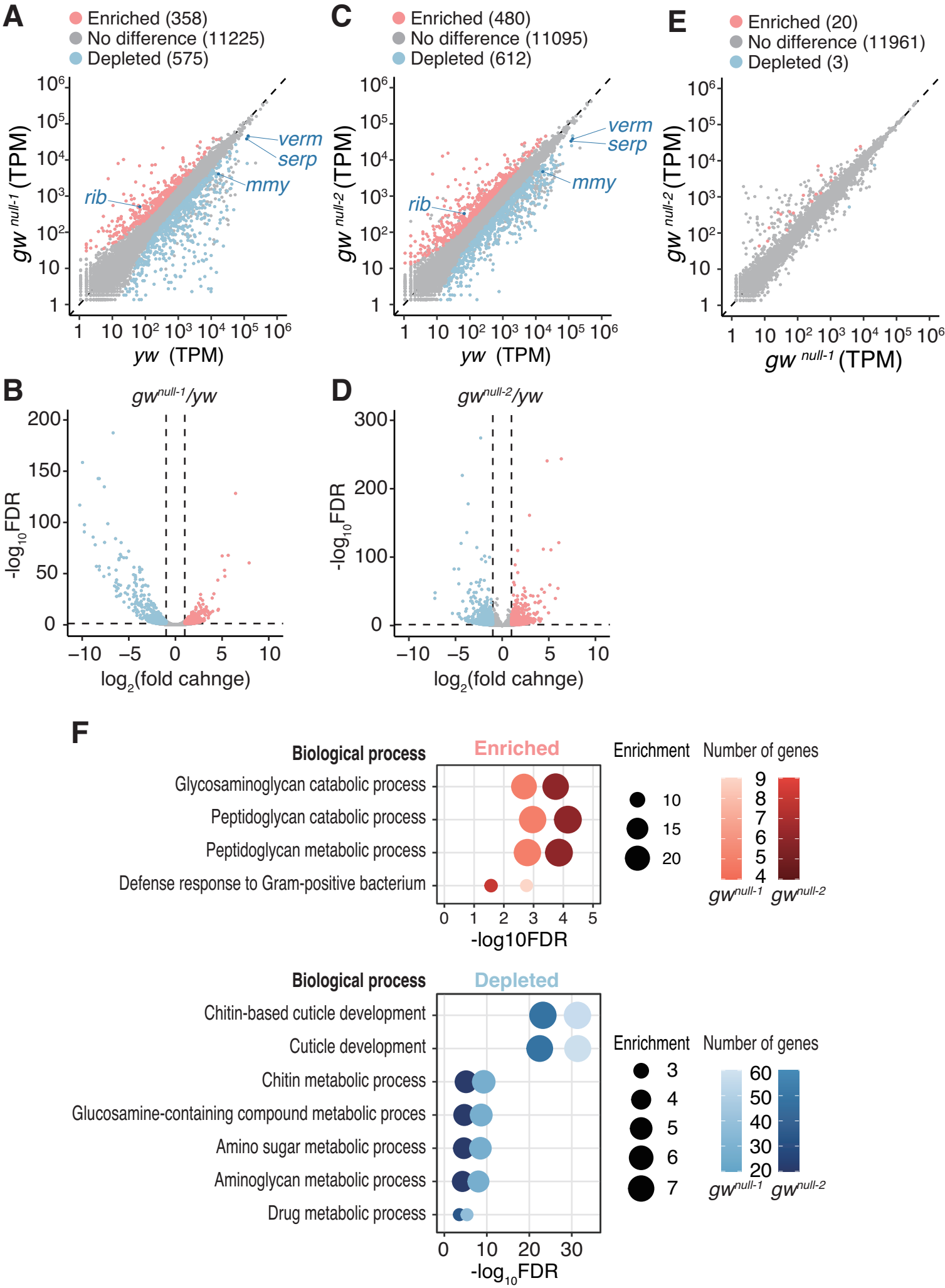

Matsuura-Suzuki et al.

Figure 7

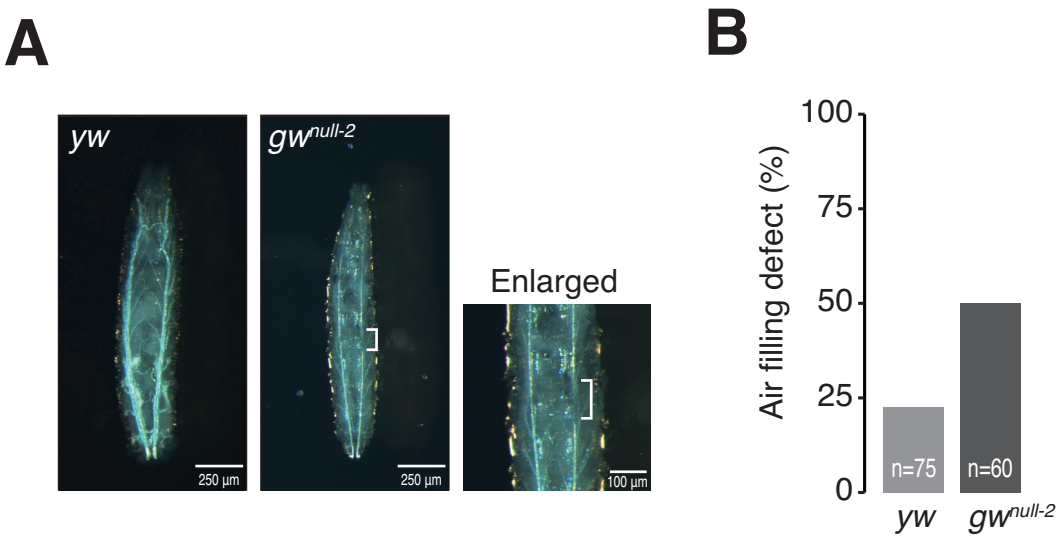
A
yw
gwnull-2
Enlarged
250 µm
250 µm
100 µm
B
Air filling defect (%)
100
75
50
25
0
n=75
n=60
yw
gwnull-2